universe

MDPI

Article

Radio Pulsars in an Electromagnetic Universe

Javlon Rayimbaev [1,2,3,4,5,6,*], Shokhzod Jumaniyozov [4,7], Maksud Umaraliyev [8] and Ahmadjon Abdujabbarov [1,3,4,7]

[1] Ulugh Beg Astronomical Institute, Astronomy Street 33, Tashkent 100052, Uzbekistan
[2] College of Engineering, Akfa University, Kichik Halqa Yuli Street 17, Tashkent 100095, Uzbekistan
[3] Power Engineering Faculty, Tashkent State Technical University, Tashkent 100095, Uzbekistan
[4] Faculty of Physics, National University of Uzbekistan, Tashkent 100174, Uzbekistan
[5] Institute of Fundamental and Applied Research, National Research University TIIAME, Kori Niyoziy 39, Tashkent 100000, Uzbekistan
[6] Institute of Engineering Physics, Samarkand State University, University Avenue 15, Samarkand 140104, Uzbekistan
[7] Institute of Nuclear Physics, Ulugbek 1, Tashkent 100214, Uzbekistan
[8] Namangan Engineering-Construction Institute, Islam Karimov Street 12, Namangan 160103, Uzbekistan
* Correspondence: javlon@astrin.uz

Abstract: The vacuum and plasma magnetosphere of neutron stars (NSs) in an electromagnetic universe (EU) were studied. First, we found vacuum solutions of the Maxwell equation for the electromagnetic field of rotating magnetized NSs in the slow-rotation approximation and analyzed the effects of the EU parameter on magnetic field components. It has been shown that in the presence of the EU field, the magnetic field lines near the star become denser and stronger compared with the case of GR. The Goldreich–Julian (GJ) charge density as a source of induced electric field was calculated. Our analyses showed that the GJ charge density increases with the increase in the EU parameter, while the size of the polar cap of NSs decreases. The solutions of Poisson equation for the scalar electric field have also been obtained at near and far zones. It has been shown that the parallel accelerating electric field increases in presence of the EU. We have also analyzed the effects of the EU on the death line for radio pulsars and shown that the position of the death line in the $P-\dot{P}$ diagram shifts up. Finally, we investigated the energy losses of rotating NSs due to electromagnetic radiation. It was obtained that at a critical value of the EU parameter, which depends on the compactness parameter, the luminosity of electromagnetic radiations of magnetospheric radiation increases about 10^6 times.

Keywords: magnetic fields; neutron stars; plasma magnetosphere; electromagnetic universe

PACS: 04.50 h; 04.40 Dg; 97.60 Gb

check for updates

Citation: Rayimbaev, J.; Jumaniyozov, S.; Umaraliyev, M.; Abdujabbarov, A. Radio Pulsars in an Electromagnetic Universe. *Universe* **2022**, *8*, 496. https://doi.org/10.3390/universe8100496

Academic Editor: Denis Leahy

Received: 10 August 2022
Accepted: 15 September 2022
Published: 22 September 2022

Publisher's Note: MDPI stays neutral with regard to jurisdictional claims in published maps and institutional affiliations.

Copyright: © 2022 by the authors. Licensee MDPI, Basel, Switzerland. This article is an open access article distributed under the terms and conditions of the Creative Commons Attribution (CC BY) license (https://creativecommons.org/licenses/by/4.0/).

1. Introduction

It is believed that NSs are rotating magnetized compact relativistic gravitational objects, being remnants of supernovae in star evolutions with an initial mass of about 8–10 $M_\odot$. Despite NSs having been discovered theoretically in 1932, they were first found in astronomical observations as a radio pulsar in 1967 [1]. After that, theoretical studies of NSs physics became the most important issue, in particular, the issue about the source of their electromagnetic radiation. For the first time, it is suggested that the source must be their kinetic energy, i.e., as a pulsar radiate, it loses its kinetic energy. In other words, kinetic energy turns into electromagnetic energy [2,3].

The feature of the electromagnetic field of dipolar magnetized NSs have been studied first in ref. [4] in Newtonian gravity using vacuum solutions of Maxwell's equations; so far, the studies have been developed by numerous authors in the frame of various gravity theories [5–13].

In fact, an NS with a strong magnetic field and fast rotation generates an induced electric field and it causes to pull out and accelerate charged particles (electrons) near the surface of the star up to ultrahigh energies. The accelerated electrons radiate high-energy photons, in turn, the photons create electron positron pairs. Consequently, the close environment of the NS fills out by plasma magnetosphere. The idea, for the first time, has been suggested by Goldreich and Julian [14]. The pulsar electrodynamics and energetic processes in the plasma magnetosphere have been developed by a number of authors in the framework of alternative theories of gravity, including general relativity [15–28].

The extension of Einstein's gravity theory known as general relativity (GR) is a useful approach in building a unique theory of interactions. Any modifications of GR and its consequences may help to deeply understand the coupling of the general relativistic effects with fields due to injected modifications. One of this kind of attempts has been proposed in [29]. Authors have unified two solutions: Schwarzschild and Bertotti–Robinson (BR) [30]. This unified solution has a simple physical interpretation: the spacetime metric describes Schwarzschild compact objects embedded in an external electromagnetic (EM) BR universe. The solution has been obtained by solving Einstein–Maxwell field equations, while the Schwarzschild and Bertotti–Robinson solutions have been used as limiting cases. The solution can be easily transformed to the Reissner–Nordström solution using the Birkhoff theorem. Mathematically, the solution represents the interpolation of two exact solutions of Einstein–Maxwell equations. The geodesic structure of a Schwarzschild black hole in an electromagnetic universe has been studied in ref. [31].

In this paper, we planned to study the observable properties of the slowly rotating neutron star described by the Schwarzschild–Bertotti–Robinson solution. In Section 2, we review Maxwell's equation in the background of S–BR spacetime. Section 3 is devoted to the study of Goldreich–Julian charge density around slowly rotating neutron stars. The solution of the Poisson equation containing Goldreich–Julian charge density is considered, and the exact solutions of the Poisson equation for scalar electric fields parallel to magnetic field lines are obtained in Section 4. Section 5 is devoted to the analysis of the death line of pulsars described by the S–BR solution. Energy loss due to the electromagnetic radiation of neutron stars described by the S–BR spacetime is analyzed in Section 6. We summarize and conclude our results in Section 7.

In this paper, we use the spacetime signature $(-,+,+,+)$ and geometrized units system $G_N = c = 1$ (only in astrophysical applications, we use the speed of light explicitly in our expressions). Latin indices run 1–3, but Greek ones 0–3.

2. Solution of Maxwell'S Equations for Stationary Magnetic Fields around Rotating Dipolar Magnetized NSs in the Electromagnetic Universe

We first derive the Maxwell equations for electromagnetic fields around a magnetized NS in an electromagnetic universe. Then, we may obtain exact solutions for magnetic field components in a vacuum case, which help to study energetic processes in the plasma magnetosphere surrounding the star. Then, we analyze the effects of the EU parameter on magnetic field structure around the NS.

2.1. Spacetime around NSs in the Electromagnetic Universe

One may estimate the ratio of spin parameter a_* and mass of an NS M in the following form

$$\frac{a_*}{M} = \frac{J}{M^2 c} \simeq \frac{1}{15}\left(\frac{P}{1\ \mathrm{ms}}\right)^{-1}\left(\frac{M}{1.4 M_\odot}\right)^{-1}\left(\frac{R}{10\ \mathrm{km}}\right)^{2},$$

where R is the radius of NS, $J = I\Omega$, I and $\Omega = 2\pi/P$ are the angular momentum, moment of inertia and angular velocity of the NS with the rotating period P, respectively. One may also estimate the value of the square of the dimensionless spin parameter a_*/M for fast-rotating NSs observed as millisecond pulsar and obtain the value $\sim$0.004. Due to

the small value of the spin parameter, we can apply slow rotation approximation to the spacetime around NSs.

The spacetime around slowly rotating NSs in an electromagnetic universe can be described using spherical coordinates (t, r, θ, ϕ) as [31]

$$ds^2 = -N^2 dt^2 + N^{-2} dr^2 + r^2(d\theta^2 + \sin^2\theta[d\phi^2 - 2\omega dt d\phi)] \,,$$

with the metric function

$$N^2 = 1 - \frac{2M}{r} + \frac{(1-a^2)M^2}{r^2}, \qquad r \geq R, \tag{1}$$

where a is the EU parameter. The frame-dragging angular velocity in the electromagnetic universe is

$$\omega = \frac{2J}{r^3}\left[1 - (1-a^2)\frac{M}{2r}\right] \tag{2}$$

For $a = 1$, the spacetime metric (1) and the frame-dragging angular velocity (2) turn into the Kerr spacetime metric in the slow-rotation approximation [7].

In fact, the energy density of the magnetic field of the NS is much less than the gravitational one. This leads to fact that the Lorentz forces on the charged particle interior of the star can not deform its shape from the sphere. Thus, we assume that the presence of the EU field also does not change the NS's shape and $J_{\rm EU} = J_{GR} = \text{const}$. On the other hand, due to uncertainties in the measurements of the moment of inertia of NS, one may use the relation $I = \beta M R^2$, with β being a coefficient corresponding to the gravitational field around the star.

In fact, the stationary metric allows the magnetic moment of the NS to be constant in time. We also assume that the medium inside the NS is a superconductive one. On the other hand, the deformation of the NS due to its rotation is small enough and can be neglected. Moreover, we consider linear angular velocities in describing the NS's angular momentum.

2.2. An Exact Solution of Maxwell Equations for Magnetic Fields

The general relativistic form of the first and second pairs of Maxwell's equations for an electromagnetic field tensor $F^{\mu\nu}$ and its dual partner ${}^*F^{\alpha\beta} = \epsilon^{\alpha\beta\mu\nu}F_{\mu\nu}$ have the forms

$$\partial_\mu(\sqrt{-g}F^{\mu\nu}) = 4\pi\sqrt{-g}J^\nu, \qquad \partial_\mu(\sqrt{-g}{}^*F^{\mu\nu}) = 0, \tag{3}$$

where $\epsilon_{\alpha\beta\sigma\gamma}$ is the Levi-Civita symbol.

Following ref. [7], we look for the exact solutions of Maxwell's equations for the components of the magnetic fields around the star in the following anzatz:

$$B^{\hat{r}}(r,\theta,\phi) = F(r)(\cos\chi\cos\theta + \sin\chi\sin\theta\cos\phi), \tag{4}$$

$$B^{\hat{\theta}}(r,\theta,\phi) = G(r)(\cos\chi\sin\theta - \sin\chi\cos\theta\cos\phi), \tag{5}$$

$$B^{\hat{\varphi}}(r,\theta,\phi) = H(r)\sin\chi\sin\theta\,, \tag{6}$$

where the functions $F(r)$, $G(r)$ and $H(r)$ stand for the radial, angular and azimuthal magnetic field components, respectively, and χ is the inclination angle between the magnetic dipole moment and rotation axis. Now, it is easy to derive systems of differential equations for these radial functions as

$$\frac{d}{dr}\left[r^2F(r)\right] + \frac{2r}{N(r)}G(r) = 0\,, \tag{7}$$

$$\frac{d}{dr}[N(r)H(r)] + F(r) = 0\,, \tag{8}$$

$$H(r) = G(r)\,. \tag{9}$$

Introducing the compactness parameter of NS as $\epsilon = M/R$ and dimensionless radial coordinate as $\eta = r/R$, one may rewrite the lapse function (1) as

$$N^2(r) = N^2(\eta;\epsilon,a) = 1 - \frac{2\epsilon}{\eta} + (1-a^2)\frac{\epsilon^2}{\eta^2}\,. \tag{10}$$

The following second-order ordinary differential equation for the radial function $F(r)$ can be obtained using the system of differential Equations (7)–(9)

$$\frac{d}{d\eta}\left[N^2(\eta;\epsilon,a)\frac{d}{d\eta}\left(\eta^2 F\right)\right] - 2F = 0\,. \tag{11}$$

We solve Equation (11) using the method of series expansion. After some calculations, we have

$$F(\eta;\epsilon,a) = -\frac{3\mu}{4a^3\epsilon^3}\left\{\left[1-(1-a^2)\frac{\epsilon^2}{\eta^2}\right]\ln\frac{\eta-\epsilon(1+a^2)}{\eta-\epsilon(1-a^2)} + \frac{(2a^2-1)\epsilon}{\eta}\left(1+\frac{\epsilon}{\eta}\right)\right\}, \tag{12}$$

$$\begin{aligned} G(\eta;\epsilon,a) &= H(\eta;\epsilon,a) \\ &= \frac{3\mu}{4a^3\epsilon^3}\left\{N(\eta;\epsilon,a)\ln\frac{\eta-\epsilon(1+a^2)}{\eta-\epsilon(1-a^2)} + \frac{(2a^2-1)\epsilon}{\eta N^2(\eta;\epsilon,a)}\left(1-\frac{\epsilon}{\eta}\right)\right\}. \end{aligned} \tag{13}$$

The projection of magnetic field lines around NS to the $x-z$ plane, in the frame of Newtonian gravity (black solid lines), GR (blue-dashed blue lines) and EU (red large-dashed lines) model are shown in Figure 1.

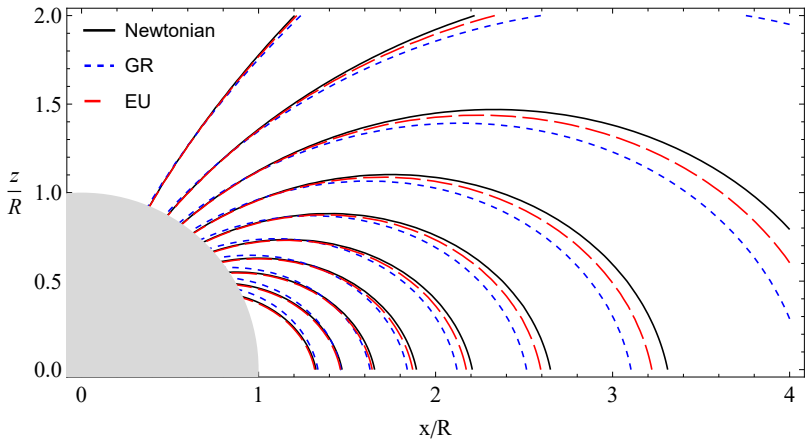


Figure 1. Profiles of magnetic field lines around a magnetized NS with compactness parameter $\epsilon = 0.2$ and inclination angle $\chi = \pi/6$ corresponding to Newtonian gravity (black line), GR (blue dashed line) and EU (red large-dashed line) model.

In order to analyze the Goldreich–Julian charge density and solve the Poisson equation for scalar electric field potential, one may write the magnetic field components in the following form:

$$B^{\hat{r}}(\eta,\theta,\phi) = \frac{B_0}{\eta^3}\frac{f(\eta)}{f(1)}(\cos\chi\cos\theta + \sin\chi\sin\theta\cos\phi)\,, \tag{14}$$

$$\begin{aligned} B^{\hat{\theta}}(\eta,\theta,\phi) &= \frac{B_0}{\eta^3}\frac{N(\eta;\epsilon,a)}{K(\eta;\epsilon,a)}\left[\frac{3}{2f(1)N^2(\eta;\epsilon,a)} - \frac{f(\eta)}{f(1)}\right] \\ &\times (\cos\chi\sin\theta - \sin\chi\cos\theta\cos\phi)\,, \end{aligned} \tag{15}$$

$$B^{\hat{\varphi}}(\eta,\theta,\phi) = \frac{B_0}{\eta^3}\frac{N(\eta;\epsilon,a)}{K(\eta;\epsilon,a)}\left[\frac{3}{2f(1)N^2(\eta;\epsilon,a)} - \frac{f(\eta)}{f(1)}\right]\sin\chi\sin\theta\,, \tag{16}$$

where $B_0 = 2\mu/R^3$ is the Newtonian value of the surface magnetic field of the NS, μ is the magnetic dipole moment of the NS and

$$f(\eta) = -3\left(\frac{\eta}{\epsilon\sqrt{2-a^2}}\right)^3\left[\frac{\sqrt{2-a^2}\epsilon}{\eta}\left(1+\frac{\epsilon}{2\eta}\right)+Kln\left(\frac{2\eta-\epsilon-\sqrt{2-a^2}\epsilon}{2\eta-\epsilon+\sqrt{2-a^2}\epsilon}\right)\right]. \quad (17)$$

In the general relativistic limit [15,32], we obtain

$$\lim_{a\to 1} f(\eta) = -3\left(\frac{\eta}{\epsilon}\right)^3\left[\ln\left(1-\frac{\epsilon}{\eta}\right)+\frac{\epsilon}{\eta}\left(1+\frac{\epsilon}{2\eta}\right)\right], \quad (18)$$

We test the effects of the EU parameter on the magnetic field of NSs using Figure 2. Figure 2 shows the radial dependence of the magnetic field components on the polar cap of the neutron star normalized to its surface magnetic field calculated in Newtonian gravity.

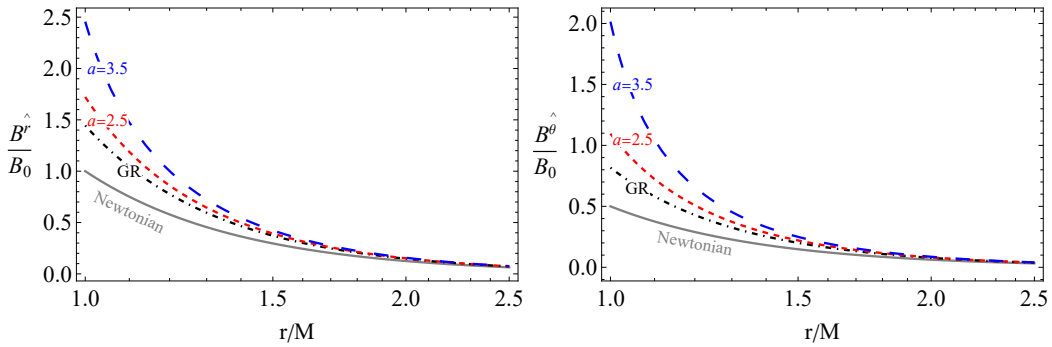


Figure 2. Radial (left panel) and angular (right panel) components of the magnetic field in the polar cap region of an NS with $\epsilon = 0.2$ normalized to its value in the Newtonian frame on the surface of the star for different values of the EU parameter.

3. Goldreich–Julian Charge Density

This section is devoted to study the plasma magnetosphere around slowly rotating NSs in the EU. Here, we assume the NS is a rotating magnetic dipole that induces an electric field by an induced electric charge in the region close to the surface of the NS.

The induced charges around the NS will be accelerated due to the presence of Lorentz force. Consequently, the accelerated charges radiate high-energy electromagnetic waves/γ rays, in turn, these γ rays produce pairs of electron–positrons. As a result, one may observe the cascade generation of positron–electron pairs. Small parts of the pairs will be recombined, however, in the vicinity of the NS, the charges will be separated due to the frame-dragging effect [33]. Then, the NS will be surrounded by quasi-neutral plasma consisting of electrons and positrons, with a specific charge distribution called the Goldreich–Julian charge [14,34,35]. Thus, the charges induce an electric field parallel to the magnetic field lines near the surface, causing them to accelerate along the file lines and create the pulsar jets from the polar cap region of the NS.

The general form of the Goldreich–Julian charge density $\rho_{\rm GJ}$ has the following form [15]

$$\rho_{\rm GJ} = -\frac{1}{4\pi}\vec{\nabla}\cdot\left(\frac{1}{N(\eta;\epsilon,a)}\vec{g}\times\vec{B}\right), \quad (19)$$

where, $g_i = -g_{0i}/g_{00}$ is a vector that can be found from the spacetime metric in Equation (1).

Following ref. [15], we have

$$\rho_{\rm GJ} = -\frac{1}{4\pi}\vec{\nabla}\cdot\left\{\frac{1}{N(\eta;\epsilon,a)}\left[1-\frac{\kappa}{\eta^3}\left(1-(a^2-1)\frac{\epsilon}{2\eta}\right)\right]\vec{g}\times\vec{B}\right\}, \quad (20)$$

with $\kappa = \epsilon\beta$ and $\vec{u} = \vec{\Omega}\times\vec{r}$,

In this work, we are interested in finding the Goldreich–Julian charge density in the polar cap region. Thus, one may easily use the small polar angle approximation as $\xi \ll 1$. Substituting Equations (14) and (15) into Equation (20), and performing several algebraic transformations, one can easily obtain the expression for the Goldreich–Julian charge density $\rho_{\rm GJ}$ in an EU in the following form

$$\begin{aligned}\rho_{\rm GJ} &= \frac{\Omega B_0}{2\pi c}\frac{1}{\eta^3}\frac{1}{N(\eta;\epsilon,a)}\frac{f(\eta;\epsilon,a)}{f(1;\epsilon,a)}\left\{\left[1-\frac{\kappa}{\eta^3}\left(1-(a^2-1)\frac{\epsilon}{2\eta}\right)\right]\cos\chi\right.\\ &+ \left.\frac{3}{2}\mathcal{H}(\eta;\epsilon,a)\cos\theta\sin\chi\cos\phi\right\}, \end{aligned} \tag{21}$$

where

$$\begin{aligned}\mathcal{H}(\eta;\epsilon,a) &= \left(1+(a^2-1)\frac{\epsilon^2}{4\eta^2}\right)^{-1}\left\{\frac{\epsilon}{\eta}\left[1-(a^2-1)\frac{\epsilon}{\eta}\right]\right.\\ &- \frac{\kappa}{\eta^3}\left[1+(a^2-1)\frac{2\epsilon}{3\eta}\left(1+\frac{\epsilon}{\eta}-(a^2-1)\frac{\epsilon^2}{2\eta^2}\right)\right]\\ &+ \left.\frac{1}{N^2(\eta;\epsilon,a)f(\eta;\epsilon,a)}\left[1+\frac{\kappa}{\eta^3}-\frac{\epsilon}{\eta}\left(3-(a^2-1)\frac{\epsilon(1-5\eta^2)}{5\eta^3}\right)\right]\right\}. \end{aligned} \tag{22}$$

One can easily see from Equation (21) and the function (22) that at the GR limit the GJ charge density takes the form obtained in ref. [15].

In Figure 3, we show the GJ charge density normalized to its Newtonian value as a function of the radial coordinate, for different values of the EU parameter a and for noninclined NSs. It is observed from the figure that an increase in the EU parameter leads the GJ charge density in the region close to the NS surface to be higher. However, at far distances of about two NS radii, the EU effects vanish.

Now, we calculate the magnetic flux coming from the NS surface using the following expression [15]

$$\Psi(\eta) = \frac{\pi R^2 B_0}{\eta}\frac{f(\eta)}{f(1)}\,. \tag{23}$$

The conservation of the magnetic flux is

$$\Psi(\eta)\sin^2\theta = \Psi(1)\sin^2\theta_0\,, \tag{24}$$

where θ_0 is the magnetic colatitude of field lines coming from the NS surface. The relationships between θ and θ_0 have the following form [15]

$$\begin{aligned}\theta(\eta) &= \xi\Theta(\eta)\\ &= \sin^{-1}\left[\sin(\xi\Theta_0)\sqrt{\eta\frac{f(1)}{f(\eta)}}\right], \end{aligned} \tag{25}$$

$$\Theta(\eta) = \Theta_0\sqrt{\eta\frac{f(1)}{f(\eta)}}\,, \tag{26}$$

where we introduced the dimensionless variable η, which takes values in the range from 0 to 1, Θ is an angle between the radius vector of the last open field line and rotation axes, and Θ_0 is the angle corresponding to the surface of the NS. One may define the angle corresponding to the surface of the NS as

$$\sin^2\Theta_0 = \frac{R}{R_{\rm LC}} \tag{27}$$

with $R_{\rm LC} = c/\Omega$ being the radius of the light-cylinder, where the velocity of the co-rotating magnetic field lines equal to the speed of light.

In Figure 4, we present the dependence of the polar cap size of an NS from the EU parameter. Here, we fixed $\epsilon = 0.15$, 0.2 and 0.25. Apparently, the polar cap significantly shrinks with the increase in the EU parameter.

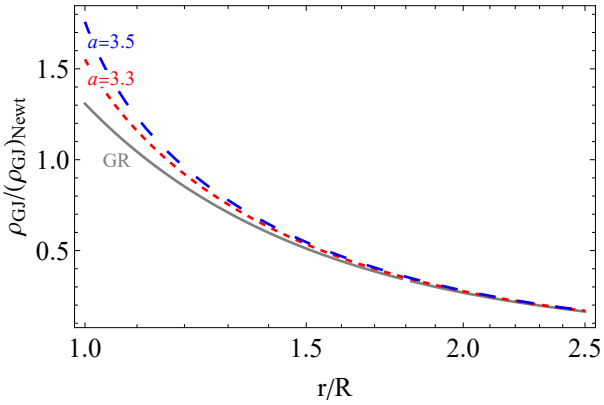


Figure 3. The ratios of the GJ charge density in the frame of EU and GR for different values of the EU parameter a and a fixed value of the compactness of the NS $\epsilon = 0.2$ and the inclination angle $\chi = 0$.

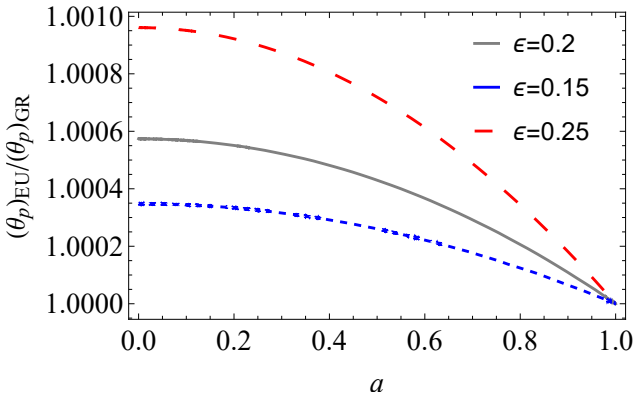


Figure 4. The angle Θ of the polar cap region of NSs as a function of the EU parameter for various values of ϵ.

4. Solutions of Poisson Equations

In this section, we solve the Poisson equation for the scalar electric potential Φ around rotating the NS in the frame of an EU. Here, we consider that magnetic field lines around the NS co-rotate as stationary with the star (see, e.g., [15,32])

$$\nabla \cdot \left(\frac{1}{N} \nabla \Phi \right) = -4\pi(\rho - \rho_{\rm GJ}) \,, \tag{28}$$

where the difference of space and GJ charge densities, $\rho - \rho_{\rm GJ}$, is called the effective space charge density, and it is the source of the unscreened electric field $E_{\parallel}$ that is parallel to magnetic field lines on the polar cap of the NS.

The general form of expression for the charge density ρ in close regions of an NS surface has the form of [15,32]:

$$\rho = \frac{\Omega B_0}{2\pi c} \frac{1}{\eta^3 N(\eta;\epsilon,a)} \frac{f(\eta)}{f(1)} \left[C(\xi)\cos\chi + D(\xi)\sin\chi\cos\phi \right] ,$$

where $C(\xi)$ and $D(\xi)$ are the functions of ξ corresponding to the boundary conditions. In order to solve the Poisson Equation (28), we introduce the dimensionless scalar function $\mathcal{F} = \eta\Phi/\Phi_0$, where $\Phi_0 = B_0\Omega R^2$, then we rewrite it in the small-angle approximation as

$$\begin{aligned}
&\frac{\partial^2\mathcal{F}}{\partial\eta^2} + \frac{1}{\Theta^2\eta^2N_*^2}\left[\frac{1}{\xi}\frac{\partial}{\partial\xi}\left(\xi\frac{\partial}{\partial\xi}\right) + \frac{1}{\xi^2}\frac{\partial^2}{\partial\phi^2}\right]\mathcal{F} \\
&= -\frac{2}{\eta^2N_*^2}\frac{f(\eta)}{f(1)}\left\{\left[1 - \frac{\kappa}{\eta^3}\left(1 - (a^2-1)\frac{\epsilon}{2\eta}\right) + C^*(\xi)\right]\cos\chi\right. \\
&\left. + \frac{3}{2}(\xi\Theta\mathcal{H}_*(\eta) + D^*(\xi))\sin\chi\cos\phi\right\}. \qquad (29)
\end{aligned}$$

Now, we solve Equation (29) using the method of separation of the variables. Here, we first perform the well-known Fourier–Bessel transformation, then it turns it into the system of ordinary differential equations. Below, we find an exact solution of the Equation (29) using the boundary conditions (see Appendix A)

$$\Phi(z) = 0, \qquad E_\parallel = -\Phi'(z) = 0 \qquad (30)$$

where $z = \eta - 1$ is a new radial coordinate which describes the height above the stellar surface.

4.1. Accelerating Parallel Electric Field in Near Zone

In this subsection, we solve Equation (29) in the close distances from the surface of the NS, $z \ll 1$, using the exact solutions (A10) and (A11). In fact, the electric field in the close magnetic field lines region is screened, while above the polar cap region, where the magnetic field lines region is, the parallel electric field is unscreened [15]. We have obtained the following expression for the scalar potential

$$\begin{aligned}
\Phi &= 12\frac{\Phi_0}{\eta}\kappa N(1;\epsilon,a)\Theta_0^3\left\{\left(1 + (a^2-1)\frac{2\epsilon}{3}\right)\cos\chi\right. \\
&+ \sum_{n=0}^{\infty}\frac{J_0(k_n\xi)}{k_n^4J_1(k_n)}\left[\exp\left(-\frac{k_n^2(1-\eta)}{N^2(1;\epsilon,a)\Theta_0^2}\right) - 1 + \frac{k_n^2(1-\eta)}{N^2(1;\epsilon,a)\Theta_0^2}\right]\frac{1}{2}\Theta_0\mathcal{H}(1;\epsilon,a)\delta(1;\epsilon,a) \\
&\times \left.\sum_{n=0}^{\infty}\frac{J_1(w_n\xi)}{w_n^4J_2(w_n)}\left[\exp\left(-\frac{w_n^2(1-\eta)}{N^2(1;\epsilon,a)\Theta_0^2}\right) - 1 + \frac{w_n^2(1-\eta)}{N^2(1;\epsilon,a)\Theta_0^2}\right]\sin\chi\cos\phi\right\}, \qquad (31)
\end{aligned}$$

and we found the corresponding parallel electric field in the following form:

$$\begin{aligned}
E_\parallel &= -12E_{\rm vac}\kappa\Theta_0^2\left\{\left(1 + (a^2-1)\frac{2\epsilon}{3}\right)\cos\chi\sum_{n=0}^{\infty}\frac{J_0(k_n\xi)}{k_n^4J_1(k_n)}\left[1 - \exp\left(\frac{k_n^2(\eta-1)}{N^2(1;\epsilon,a)\Theta_0^2}\right)\right]\right. \\
&+ \left.\frac{1}{2}\Theta_0\mathcal{H}(1;\epsilon,a)\delta(1;\epsilon,a)\sin\chi\cos\phi\sum_{n=0}^{\infty}\frac{J_1(w_n\xi)}{w_n^4J_2(w_n)}\left[1 - \exp\left(\frac{w_n^2(\eta-1)}{N^2(1;\epsilon,a)\Theta_0^2}\right)\right]\right\}, \qquad (32)
\end{aligned}$$

where $\delta(\eta;\epsilon,a) = d\ln[\Theta(\eta;\epsilon,a)H(\eta;\epsilon,a)]/d\eta$, and $E_{\rm vac} = (\Omega R/c)B_0$ is the Newtonian value of the surface electric field induced by rotation of the neutron star with angular velocity Ω in vacuum [4].

4.2. The Parallel Electric Field in Far Zone

The region lying on the distances larger than the polar cap size but too far from the light cylinder is called far zone, $\Theta_0 \ll \eta - 1 \ll R_{LC}/R$. The expressions for the potential and the parallel electric field in this zone obtain the form as [15]

$$\Phi = \Phi_0\Theta_0^2\frac{1-\xi^2}{2}\left\{\kappa\left[1-\frac{1}{\eta^3}+(a^2-1)\frac{\epsilon}{2}\left(1-\frac{1}{\eta^4}\right)\right]\cos\chi + \frac{3}{4}\Theta_0\mathcal{H}(1;\epsilon,a)\left(\frac{\mathcal{H}(\eta;\epsilon,a)\Theta(\eta;\epsilon,a)}{\mathcal{H}(1;\epsilon,a)\Theta_0}-1\right)\xi\sin\chi\cos\phi\right\}, \quad (33)$$

and

$$E_{\parallel} = -\frac{3}{2}E_{\rm vac}\Theta_0^2(1-\xi^2)\left\{\frac{\kappa}{\eta^4}\left(1+(a^2-1)\frac{2\epsilon}{3\eta}\right)\cos\chi + \mathcal{H}(\eta;\epsilon,a)\Theta(\eta;\epsilon,a)\delta(\eta;\epsilon,a)\xi\sin\chi\cos\phi\right\}, \quad (34)$$

In Figure 5, we present the parallel electric field corresponding to the acceleration of charged particles along the field line as a function of the radial coordinate for different values of the EU parameter a.

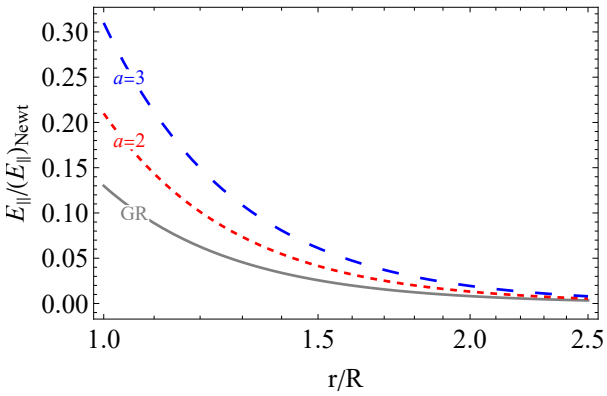


Figure 5. The radial r/R dependence of normalized values of the parallel electric fields in the EU and in GR to its Newtonian value for different values of the parameter a when compactness of the star $\epsilon = 0.2$.

5. Death Line of Radio Pulsars

In this section, we investigate the death line condition for radio pulsars in the EU. Mathematically, the death line condition is a relationship between period and period derivative of pulses from pulsars and/or the surface magnetic field of a pulsar and its period. On the other hand, the condition defines whether a pulsar emits electromagnetic radiations or not. In other words, if a pulsar is visible, it means that its position in the $P-\dot{P}$ diagram lies on and/or above the death line, otherwise, it would not be observed. In real astrophysical observations, when a visible pulsar goes out from observations, that means the position of the pulsar shifts downward below the death line. For example, part-time pulsars present a similar cycle quasi periodically.

In fact, the radiation of NSs is connected with energetic processes in the plasma magnetosphere of the NSs, such as the cascade pair production. In fact, when the energy of primary accelerated charged particles (electrons and/or positrons) is not high enough to produce high energetic photons that allow generating secondary electron–positron pairs, the cascade process cannot develop anymore. It may happen when the surface magnetic field is weak and/or the NS rotates slowly.

$$B_0 \sim \kappa\left(\frac{P}{1\text{s}}\right)^{7/2}\left(\frac{R}{10\text{km}}\right)^{-3}10^{12}\text{G}\,. \quad (35)$$

According to the plasma magnetospheric models, the mechanism of pulsar radiation connects with electromagnetic waves generated by the accelerating electrons (and/or positrons) along the open magnetic field lines during their cascade form of pair productions. To generate the secondary electron–positron pair production in the plasma magnetosphere of the NS, its surface magnetic field has to be [36]:

$$B_{\rm cr} \geq B_{\rm surf} \geq B_{\rm DL}\,, \tag{36}$$

where

$$B_{\rm surf} = 6.4 \times 10^{19}\sqrt{P\dot{P}}, G \tag{37}$$

is the surface magnetic field, and it can be found using observational data of pulsars such as pulse period and period derivative. $B_{\rm cr}$ is a critical value for the magnetic field's so-called quantum Schwinger limit $B_{\rm Schw} = m^2c^3/e\hbar \approx 4.4 \times 10^{13}$ G, corresponding to the threshold magnetic field where the cyclotron energy of electron is equal to the energy of electrons at rest. Consequently, $B_{\rm DL}$ is the minimum value of the magnetic field defining the so-called "death line" regime, which switches off the pair production.

Here, we consider the radiation of electromagnetic waves produced by the inverse Compton scattering process. In this case, the intensity of the radiations depends on the Lorentz factor of accelerating charged particles, electrons and/or positrons by parallel electric field near the NS surface [37]

$$\gamma = \frac{e\Phi}{mc^2} = \frac{10^6}{P^2}\left(\frac{B}{10^{12}{\rm G}}\right)\left\{1 - \frac{1}{\eta^3} - (a^2-1)\frac{\epsilon}{2}\left(1 - \frac{1}{\eta^4}\right)\right\}. \tag{38}$$

As a simple case, here, we consider noninclined, rotating $\chi = 0$. To calculate the death line condition for radio pulsars, we follow ref. [37].

It can be obtained from the expression for the case of inverse Compton scattering by energetic electrons/positrons in the following form [37],

$$\begin{aligned} S_{\rm ph} &= \frac{(1.5\eta)^3 10^2 P^{5/2}}{5\left[1 - \frac{1}{\eta^3} + (a^2-1)\frac{\epsilon}{2}\left(1 - \frac{1}{\eta^4}\right)\right]}\left(\frac{B}{10^{12}{\rm G}}\right)^{-2} \\ &= \frac{\eta}{2}10^6\,, \end{aligned} \tag{39}$$

One may immediately have

$$\begin{aligned} 74\left(\frac{B}{10^{12}{\rm G}}\right)^2 P^{-5/2} &= \frac{\eta^2}{1 - \frac{1}{\eta^3} - (a^2-1)\frac{\epsilon}{2}\left(1 - \frac{1}{\eta^4}\right)} \\ &= \mathcal{D}(\eta, \epsilon, a)\,, \end{aligned} \tag{40}$$

where the function $\mathcal{D}(\eta, \epsilon, a)$ corresponds to characterize the death line condition, and it is the function of the radial coordinate and impact parameter, including the EU parameter.

The function $\mathcal{D}(\eta, \epsilon, a)$ takes a maximum value at a critical distance which corresponds to the maximum distance from the NS center, where the secondary plasma formation cuts off. One can find the critical distance solving the following equation with respect to the radial coordinate η:

$$\frac{d}{d\eta}\mathcal{D}(\eta, \epsilon, a) = 0\,. \tag{41}$$

In this case, it is quite a long form of $\eta_{\rm cr}$ to express analytically. That is why we provide graphical analyses.

In Figure 6, we show the dependence of the critical distance on the EU parameter for various values of the compactness parameter. It is observed from the figure that the critical distance decreases with increasing the parameter a. In the absence of the EU parameter ($a = 0$), the distance takes the value $\eta_{\rm cr} \simeq 1.35$, as it was obtained in ref. [37].

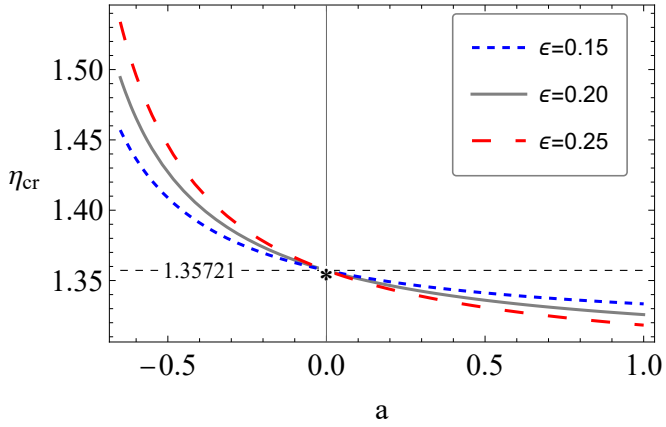


Figure 6. The critical distance η_{cr} as a function of the EU parameter a for various values of the compactness parameter.The symbol * implies general relativistic case.

In Figure 7, we show relationships between the function $\mathcal{D}$ and the EU parameter for different values of the compactness parameter of NSs. It is seen from the figure that an increase in a causes the maximum of $\mathcal{D}$ to decrease.

Now, one can derive the death line condition using Equations (37) and (40) together with the numerical solutions of Equation (41), numerically, and show the effects of the EU parameter on the position of the death line in the $P - \dot{P}$ diagram.

The death line position for radio pulsars immersed in an EU in the $P\dot{P}$ diagram is illustrated in Figure 8. The points A, B and C stand for the pulsars J 2145-0750 with the period $P = 16.052$ ms and slowdown rate $\dot{P} = 2.98 \times 10^{-20}$ s $\cdot$ s^{-1}, J 0024-7204 D (P = 5.35757 ms, $\dot{P} = 3.429 \times 10^{-21}$ s $\cdot$ s^{-1}) and J 0024-7204 H (P = 3.21 ms, $\dot{P} = 1.83 \times 10^{-21}$ s $\cdot$ s^{-1}), respectively [38,39]. In fact, according to the definition of the death line condition, a pulsar can be observable when its potion in the $P - \dot{P}$ diagram lies over/on the death line. In order to obtain upper values of the EU parameter, we may assume the pulsars lie on the death line in the EU. This implies that if the EU parameter exceeds the upper value, the pulsar becomes invisible. One may numerically calculate the upper values for the above-mentioned pulsars using their observational data, such as rotation period and period derivatives. It is shown that the upper limit values are different for each of the pulsars depending on their observational parameters. Our numerical analysis shows that the upper limit for the pulsar J 2145-0750 is $a_u \simeq 2.55999$, while for the pulsars J 0024-7204 D and J 0024-7204 H, $a_u \simeq 4.2844$ and $a_u \simeq 1.8633$. One can observe from the diagram that in the presence of the EU parameter, the death line for the radio pulsars shifts up due to the increase in the surface magnetic field.

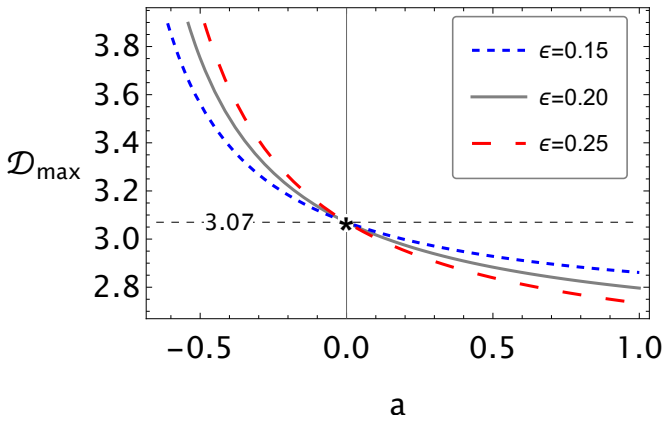


Figure 7. Maximum values of $\mathcal{D}$ as a function of the EU parameter for several values of the compactness parameter of NSs. The symbol * implies general relativistic case.

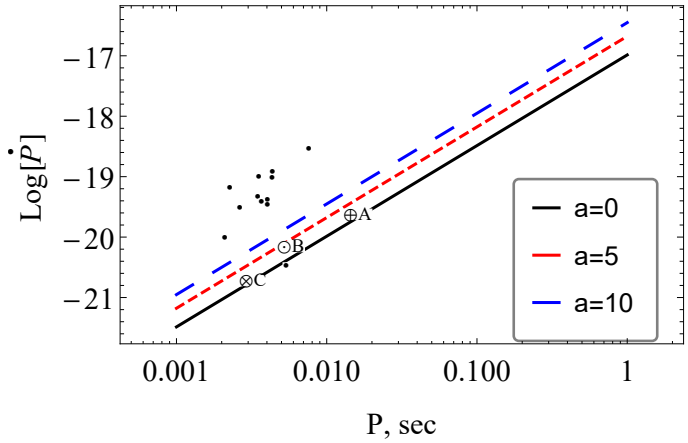


Figure 8. Position of the death line for NSs in the $P\dot{P}$ space for various values of the EU parameter and the fixed value of compactness parameter $\epsilon = 0.2$. A, B and C points imply the positions of pulsars J 2145-0750, J 0024-7204 D and J 0024-7204 H, respectively.

6. Energy Losses

In this section, we consider the electromagnetic radiation of NSs by (i) magnetodipolar radiation for inclined NSs and (ii) radiations of accelerating charged particles (electrons and positrons) in the plasma magnetosphere of NSs along open field lines coming from the polar cap of the star that may cause the formation of pulsar jets. In fact, the dynamics of charged particles in the plasma magnetosphere is much more complex.

6.1. Energy Losses by Magnetodipolar Radiations

Here, we calculate of luminosities of the inclined magnetized NSs through pure magnetodipolar radiation in the EU as [27]

$$\mathcal{L}_{\rm em} = \frac{\Omega_0^4 R^6 B_0^*}{6c^3} \sin^2\chi \tag{42}$$

where $\Omega_0 = \Omega/N(1;\epsilon,a)$ is the angular velocity of the NS at its surface, and $B_0^* = B_0 f(1;\epsilon,a)$ is the surface magnetic field of the NS measured by an observer located in the frame of reference in the EU.

The luminosity in Newtonian gravity [40]

$$(\mathcal{L}_{\rm em})_{\rm Newt} = \frac{\Omega^4 R^6 B_0^2}{6c^3} \sin^2\chi\,. \tag{43}$$

In Figure 9, we show the effects of the EU parameter on magnetodipolar radiations of inclined dipolar magnetized NSs. It is observed from the figure that the luminosity decreases with the increase in the EU parameter, and it increases more slowly with respect to the increase in ϵ in the EU than it does in GR. Consequently, the presence of the EU field causes faster slowing down of a pulsar, and it can be an explanation of the shifting of the death line of radio pulsars upward, causing them to suddenly become invisible. Because, according to rotation-powered pulsar models, which explain that the source of the electromagnetic radiations of pulsars is their rotational energy, as the luminosity equals the rotational kinetic energy losses [27],

$$\mathcal{L}_{\rm em} = -\frac{dE_{\rm kin}}{dt}\,. \tag{44}$$

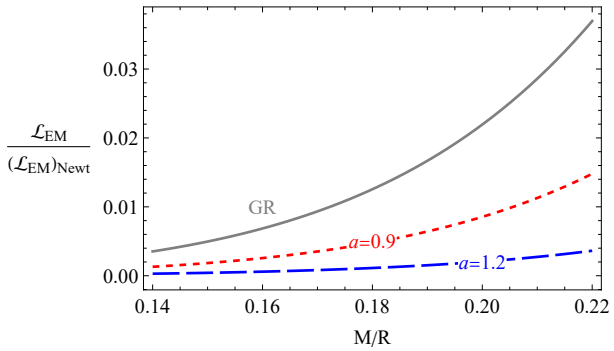


Figure 9. Normalized values of the magnito-dipolar radiation luminosity to its Newtonian value for different values of the EU parameter.

This means the radiation forces slow down the pulsar as

$$\frac{dE_{\rm kin}}{dt} = -\frac{4\pi^2 I}{P^3}\frac{dP}{dt}. \tag{45}$$

Inertia moment I in spherical coordinates can be calculated as

$$I = \int d^3r\sqrt{\gamma}e^{-\Lambda(r)}\rho(r)r^2\sin^2\theta \tag{46}$$

and, in the Newtonian limit, the moment of inertia tends to $I_0 = (2/5)MR^2$ One may express relations between the magnetic field of a pulsar and the measurable quantity in the pulsar observations $P\dot{P}$ as

$$\begin{aligned}\left(P\dot{P}\right)_{\rm max} &= \frac{2\pi^2}{3c^3}\frac{BR^6}{N^4(1;\epsilon,a)I} \\ &= \left(\frac{f^2(1;\epsilon,a)}{N^4(1;\epsilon,a)}\frac{I_0}{I}\right)\frac{2\pi^2}{3c^3}\frac{BR^6}{I_0}\,.\end{aligned} \tag{47}$$

6.2. Energy Losses through Plasma Magnetospheric Radiations

In this subsection, we study the effect of the EU parameter on total luminosity radiations of accelerating charged particles along the open magnetic field line region in the plasma magnetosphere. It has potential applications in the theory of pulsar electrodynamics (see, e.g., [41]).

The total luminosity of the radiations can be calculated using the following expression [32]:

$$L_{\rm EM} = -2c\int\langle\rho\Phi\rangle dS\,, \tag{48}$$

where the averaging over time is by angular brackets, and the integration is over the surface across the open field line region.

The explicit form of (48) for inclined NSs has the following form [32]

$$L_{\rm EM} = \frac{3}{2}\kappa\left(1-(a^2-1)\frac{2\epsilon}{3}\right)\left[1-\kappa\left(1-(a^2-1)\frac{2\epsilon}{3}\right)\right]\dot{E}_{\rm rot}\,, \tag{49}$$

where

$$\dot{E}_{\rm rot} = \frac{1}{6}\frac{\Omega^4 B_0^2 R^6}{c^3 f^2(1;\epsilon,a)} = \frac{1}{f^2(1;\epsilon,a)}\left(\dot{E}_{\rm rot}\right)_{\rm Newt}\,, \tag{50}$$

and it is in GR ($a = 1$)

$$(L_{\rm EM})_{a=1} = \frac{3}{2}\frac{\kappa(1-\kappa)}{f^2(1;\epsilon,1)}\left(\dot{E}_{\rm rot}\right)_{\rm Newt} \tag{51}$$

The energy loss of NS is through plasma magnetospheric radiations in the frame of the EU. When $\kappa = 0.15$ (shown in [15]), the luminosity takes the form:

$$L_{\rm EM} \simeq \frac{9}{40}\dot{E}_{\rm rot}\left(1-(a^2-1)\frac{2\epsilon}{3}\right)I_{45}R_6^{-3}\left[1-\frac{3}{20}\left(1-(a^2-1)\frac{2\epsilon}{3}\right)I_{45}R_6^{-3}\right], \tag{52}$$

where $I_{45} = I/(10^{45}\ {\rm g}\cdot{\rm cm}^2)$ and $R_6 = R/(10^6\ {\rm cm})$ are normalized inertia momentum and radius of the neutron star.

In Figure 10, we show the dependence of the luminosity of plasma magnetospheric radiations of NSs in the EU normalized to its GR value on the parameter a (left panel) and compactness parameter (right panel) of the star. It is observed that there is a critical value in the value of the EU parameter; the luminosity takes the maximum, increasing about millions of times, and it is equal for typical NSs with luminosity in the order of 10^{38} erg/sec to about $\sim 10^{44}$ erg/s, which corresponds to fast radio bursts from the NS (magnetar) magnetosphere [42,43].

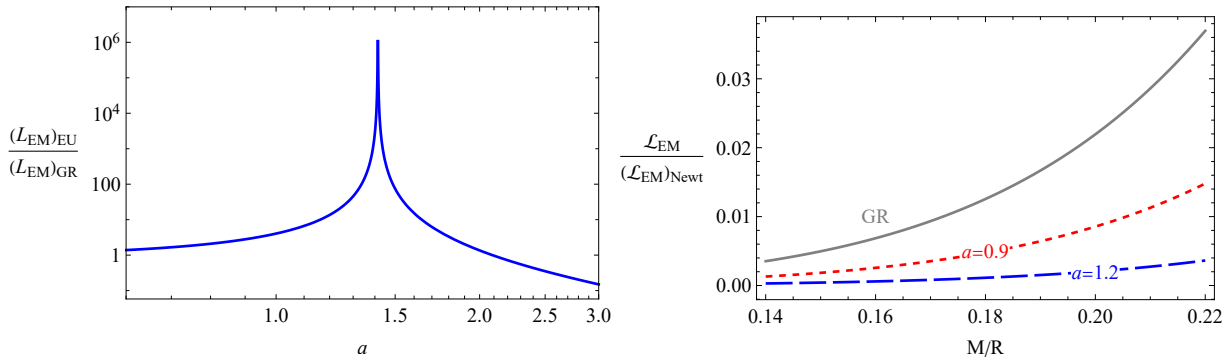


Figure 10. Plasma magnetospheric radiation luminosity in EU normalized to its GR value as a function of the EU parameter a (left panel) and the compactness ϵ (right panel).

7. Conclusions

In this paper, we studied the vacuum and plasma magnetosphere of NSs immersed in an electromagnetic universe, and the following results are obtained:

1. We found the vacuum solutions of the Maxwell equations for electromagnetic fields of slowly rotating magnetized NSs. The effects of the EU parameter on magnetic field components are obtained. It is also shown that the presence of the EU field makes the field lines denser and stronger near the star in comparison with GR.
2. We calculated the Goldreich–Julian charge density, which is responsible for the source of the induced electric field. The analyses of the effects of the EU parameter on the GJ charge density show that the charge density increases with an increase in the EU parameter.
3. The effects of the EU field on the size of the polar caps of NSs are also explored. It is found that the size decreases due to the presence of the EU.
4. Solutions of the Poisson equation for the scalar electric field, which is parallel to the magnetic field lines, are also obtained at near and far zones in small-angle approximation by separating the variables and performing the Fourier–Bessel transformations, and it is observed that the parallel accelerating electric field increases in the presence of the EU.

5. We also analyzed the effects of the EU on the death line conditions for radio pulsars, corresponding to the plasma magnetospheric radiations through inverse Compton scattering processes, and show that the position of the death line in the $P-\dot{P}$ diagram shifts up, causing a pulsar which lies on the death line to become invisible.
6. Using the death line condition for radio pulsars, and observational data from the pulsars, we found that the upper limits for the EU parameter for the pulsar J 2145-0750 is $a_u \simeq 2.55999$, while for the pulsars J 0024-7204 D and J 0024-7204 H, $a_u \simeq 4.2844$ and $a_u \simeq 1.8633$.
7. Finally, we investigated magnetodipolar and plasma magnetospheric energy losses of rotating NSs. It is obtained that with the increase in the EU parameter, the magnetodipolar radiation luminosity decreases, while the luminosity of plasma magnetospheric radiations increases sufficiently. Moreover, at a critical value of the EU parameter, the electromagnetic radiations of magnetospheric radiation increase about 10^6 times, and the critic value depends on the compactness parameter.

Author Contributions: Conceptualization, J.R. and S.J.; methodology, J.R.; software, J.R. and S.J.; validation, M.U. and A.A.; formal analysis, J.R. and A.A.; investigation, A.A. and J.R. All authors have read and agreed to the published version of the manuscript.

Funding: This research is supported by Grant F-FA-2021-510 of the Uzbekistan Ministry for Innovative Development.

Data Availability Statement: Not applicable.

Acknowledgments: J.R. thanks to the ERASMUS+ project 608715-EPP-1-2019-1-UZ- 329 EPPKA2-JP (SPACECOM).

Conflicts of Interest: The authors declare no conflict of interest.

Appendix A. Solution of Poisson Equation

We look for the general solution of Equation (29) in the following separable form [15]:

$$\mathcal{F}(\eta,\xi) = F(\eta,\xi)\cos\chi + S(\eta,\xi)\sin\chi\cos\phi \tag{A1}$$

Substituting Equation (A1) into Equation (29), we obtain the following equations for unknown functions $F(\eta,\xi)$ and $S(\eta,\xi)$ [15]:

$$\left[\frac{\partial^2}{\partial\eta^2} + \frac{1}{\eta^2 N^2\Theta^2}\frac{1}{\xi}\frac{\partial}{\partial\xi}\left(\xi\frac{\partial}{\partial\xi}\right)\right]F(\eta,\xi) = -\frac{2}{\eta^2 N^2(\eta;\epsilon,a)} \times \frac{f(\eta;\epsilon,a)}{f(1;\epsilon,a)}\left[1-\frac{\kappa}{\eta^3}\left(1-(a^2-1)\frac{\epsilon}{2\eta}\right)-C(\xi)\right], \tag{A2}$$

$$\left[\frac{\partial^2}{\partial\eta^2} + \frac{1}{\eta^2 N^2(\eta;\epsilon,a)\Theta^2}\left(\frac{1}{\xi}\frac{\partial}{\partial\xi}\left(\xi\frac{\partial}{\partial\xi}\right)-\frac{1}{\xi^2}\right)\right]S(\eta,\xi) = -\frac{3}{\eta^2 N^2(\eta;\epsilon,a)} \times \frac{f(\eta;\epsilon,a)}{f(1;\epsilon,a)}[\xi\Theta\mathcal{H}(\eta;\epsilon,a)-D(\xi)]\,. \tag{A3}$$

We use the Fourier–Bessel transformation to solve Equations (A2) and (A3) [15]

$$F(\eta,\xi) = \sum_{n=1}^{\infty} F_n(\eta)J_0(k_n\xi)\,, \qquad F_n(\eta) = \frac{2}{J_1^2(k_n)}\int_0^1 \xi F(\eta,\xi)J_0(k_n\xi)d\xi\,, \tag{A4}$$

$$S(\eta,\xi) = \sum_{n=1}^{\infty} S_n(\eta)J_1(w_n\xi)\,, \qquad S(\eta) = \frac{2}{J_2^2(w_n)}\int_0^1 \xi S(\eta,\xi)J_1(w_n\xi)d\xi\,, \tag{A5}$$

where k_n and w_n are zeros of Bessel functions of type $J_0(x)$ and $J_1(x)$, respectively. We substitute the expressions (A4) and (A5) into Equations (A2) and (A3) and obtain

$$\left[\frac{\partial^2}{\partial\eta^2} - \frac{k_n^2\Theta^{-2}}{\eta^2 N^2(\eta;\epsilon,a)}\right]F_n = -\frac{2}{\eta^2 N^2(\eta;\epsilon,a)} \times \frac{f(\eta;\epsilon,a)}{f(1;\epsilon,a)}\left\{\frac{2}{k_n J_1(k_n)}\left[1-\frac{\kappa}{\eta^3}\left(1-(a^2-1)\frac{\epsilon}{2\eta}\right)\right]-C_n\right\}, \tag{A6}$$

$$\left[\frac{\partial^2}{\partial\eta^2} - \frac{w_n^2\Theta^{-2}}{\eta^2 N^2(\eta;\epsilon,a)}\right]S_n = -\frac{3}{\eta^2 N^2(\eta;\epsilon,a)\Theta^2} \times \frac{f(\eta;\epsilon,a)}{f(1;\epsilon,a)}\left[\frac{2}{w_n J_2(w_n)}\Theta\mathcal{H}(\eta;\epsilon,a)-D_n\right]. \tag{A7}$$

C_n and D_n can be found as

$$C_n = \frac{2}{J_1^2(k_n)}\int_0^1 \xi C(\xi)J_0(k_n\xi)d\xi\,, \qquad D_n = \frac{2}{J_2^2(w_n)}\int_0^1 \xi D(\xi)J_1(w_n\xi)d\xi\,. \tag{A8}$$

To solve Equations (A6) and (A7) near the surface of an NS, we use the following boundary conditions $\Phi(0) = 0$ and $E_\parallel(0) = -\Phi'(0) = 0$, where we introduced the dimensionless height $z = \eta - 1$.

$$F(0) = 0\,, \qquad \left.\frac{F(z)}{dz}\right|_{z=0} = 0 \quad \text{and} \quad S(0) = 0\,, \qquad \left.\frac{S(z)}{dz}\right|_{z=0} = 0\,. \tag{A9}$$

Solving Equations (A6) and (A7) near the surface of the NS, we obtain [15]

$$F_n = \frac{12\kappa N(1;\epsilon,a)}{k_n^4 J_1(k_n)}\left(1+(a^2-1)\frac{2\epsilon}{3}\right) \times \left[\exp\left(-\frac{k_n^2}{N^2(1;\epsilon,a)\Theta_0^2}z\right)-1+\frac{k_n^2}{N^2(1;\epsilon,a)\Theta_0^2}z\right], \tag{A10}$$

$$S_n = \frac{6\kappa N(1;\epsilon,a)\Theta_0}{w_n^4 J_2(w_n)}H(1;\epsilon,a)\delta(1;\epsilon,a) \times \left[\exp\left(-\frac{w_n^2}{N^2(1;\epsilon,a)\Theta_0^2}z\right)-1+\frac{w_n^2}{N^2(1;\epsilon,a)\Theta_0^2}z\right]. \tag{A11}$$

References

1. Hewish, A.; Bell, S.J.; Pilkington, J.D.H.; Scott, P.F.; Collins, R.A. Observation of a Rapidly Pulsating Radio Source. *Nature* **1968**, *217*, 709–713. [CrossRef]
2. Pacini, F. Rotating Neutron Stars, Pulsars and Supernova Remnants. *Nature* **1968**, *219*, 145–146. [CrossRef]
3. Gold, T. Rotating Neutron Stars as the Origin of the Pulsating Radio Sources. *Nature* **1968**, *218*, 731–732. [CrossRef]
4. Deutsch, A.J. The electromagnetic field of an idealized star in rigid rotation in vacuo. *Ann. D'Astrophys.* **1955**, *18*, 1.
5. Muslimov, A.G.; Tsygan, A.I. Electric Fields Generated by a Rotating Neutron Star in a Vacuum with Allowance for Gtr Effects. *Sov. Astonomy* **1986**, *30*, 567.
6. Konno, K.; Kojima, Y. General Relativistic Modification of a Pulsar Electromagnetic Field. *Prog. Theor. Phys.* **2000**, *104*, 1117–1127. [CrossRef]
7. Rezzolla, L.; Ahmedov, B.J.; Miller, J.C. General relativistic electromagnetic fields of a slowly rotating magnetized neutron star—I. Formulation of the equations. *Mon. Not. R. Astron. Soc.* **2001**, *322*, 723–740. [CrossRef]
8. Rezzolla, L.; Ahmedov, B.J.; Miller, J.C. Stationary Electromagnetic Fields of a Slowly Rotating Magnetized Neutron Star in General Relativity. *Found. Phys.* **2001**, *31*, 1051–1065. [CrossRef]
9. Ahmedov, B.J.; Fattoyev, F.J. Magnetic fields of spherical compact stars in a braneworld. *Rhys. Rev. D* **2008**, *78*, 047501. [CrossRef]
10. Hakimov, A.; Abdujabbarov, A.; Ahmedov, B. Magnetic fields of spherical compact stars in modified theories of gravity: F(R) type gravity and Hořava-Lifshitz gravity. *Phys. Rev. D* **2013**, *88*, 024008. [CrossRef]
11. Turimov, B.V.; Ahmedov, B.J.; Hakimov, A.A. Stationary electromagnetic fields of slowly rotating relativistic magnetized star in the braneworld. *Phys. Rev. D* **2017**, *96*, 104001. [CrossRef]

12. Turimov, B.; Ahmedov, B.; Abdujabbarov, A.; Bambi, C. Electromagnetic fields of slowly rotating magnetized compact stars in conformal gravity. *Phis. Rev. D* **2018**, *97*, 124005. [CrossRef]
13. Rayimbaev, J.; Turimov, B.; Marcos, F.; Palvanov, S.; Rakhmatov, A. Particle acceleration and electromagnetic field of deformed neutron stars. *Mod. Phys. Lett. A* **2020**, *35*, 2050056. [CrossRef]
14. Goldreich, P.; Julian, W.H. Pulsar Electrodynamics. *Astrophys. J.* **1969**, *157*, 869. [CrossRef]
15. Muslimov, A.G.; Tsygan, A.I. General relativistic electric potential drops above pulsar polar caps. *Mon. Not. R. Astron. Soc.* **1992**, *255*, 61–70. [CrossRef]
16. Morozova, V.S.; Ahmedov, B.J. Quantum Interference Effects in Slowly Rotating Nut Space-Time. *Int. J. Mod. Phys. D* **2009**, *18*, 107–118. [CrossRef]
17. Ahmedov, B.J.; Fattoyev, F.J. Quasi-Stationary Electromagnetic Effects in Conductors and Superconductors in Schwarzschild Space-Time. *Int. J. Mod. Phys. D* **2005**, *14*, 817–835. [CrossRef]
18. Rayimbaev, J.R.; Ahmedov, B.J.; Juraeva, N.B.; Rakhmatov, A.S. Plasma magnetosphere of deformed magnetized neutron star. *Astrophys. Space Sc.* **2015**, *356*, 301–308. [CrossRef]
19. Rayimbaev, J.; Turimov, B.; Ahmedov, B. Braneworld effects in plasma magnetosphere of a slowly rotating magnetized neutron star. *Int. J. Mod. Phys. D* **2019**, *28*, 1950128. [CrossRef]
20. Rayimbaev, J.; Turimov, B.; Palvanov, S. Plasma magnetosphere of slowly rotating magnetized neutron star in branewold. *Int. J. Mod. Phys. Conf. Ser.* **2019**, *49*, 1960019. [CrossRef]
21. Ahmedov, B.J.; Khugaev, A.V.; Abdujabbarov, A.A. External electromagnetic fields of a slowly rotating magnetized star with gravitomagnetic charge. *Astrophys. Space Sci.* **2012**, *337*, 679–683. [CrossRef]
22. Ahmedov, B.J.; Abdujabbarov, A.A.; Fayzullaev, D.B. Plasma magnetosphere and spin down of rotating magnetized strange stars in general relativity. *Astrophys. Space Sci.* **2013**, *346*, 507–512. [CrossRef]
23. Ahmedov, B.J.; Morozova, V.S. Plasma magnetosphere formation around oscillating magnetized neutron stars. *Astrophys. Space Sci.* **2009**, *319*, 115–117. [CrossRef]
24. Morozova, V.S.; Ahmedov, B.J.; Zanotti, O. Explaining the subpulse drift velocity of pulsar magnetosphere within the space-charge limited flow model. *Mon. Not. R. Astron. Soc.* **2014**, *444*, 1144–1156. [CrossRef]
25. Abdikamalov, E.B.; Ahmedov, B.J.; Miller, J.C. The magnetosphere of oscillating neutron stars in general relativity. *Mon. Not. R. Astron. Soc.* **2009**, *395*, 443–461. [CrossRef]
26. Mofiz, U.A.; Ahmedov, B.J. Plasma Modes along the Open Field Lines of a Neutron Star. *Astrophys. J.* **2000**, *542*, 484–492. [CrossRef]
27. Rezzolla, L.; Ahmedov, B.J. Electromagnetic fields in the exterior of an oscillating relativistic star—I. General expressions and application to a rotating magnetic dipole. *Mon. Not. R. Astron. Soc.* **2004**, *352*, 1161–1179. [CrossRef]
28. Rezzolla, L.; Ahmedov, B.J. Electromagnetic fields in the exterior of an oscillating relativistic star—II. Electromagnetic damping. *Mon. Not. R. Astron. Soc.* **2016**, *459*, 4144–4160. [CrossRef]
29. Halilsoy, M.; Al-Badawi, A. Metric for a static mass coupled to a stationary electromagnetic field. *Class. Quantum Gravity* **1995**, *12*, 3013–3017. [CrossRef]
30. Bertotti, B. Uniform Electromagnetic Field in the Theory of General Relativity. *Phys. Rev.* **1959**, *116*, 1331–1333. [CrossRef]
31. Al-Badawi, A.; Owaidat, M.Q.; Tarawneh, S. The geodesics structure of Schwarzschild black hole immersed in an electromagnetic universe. *Int. J. Mod. Phys. D* **2017**, *26*, 1750169. [CrossRef]
32. Muslimov, A.; Harding, A.K. Toward the Quasi–Steady State Electrodynamics of a Neutron Star. *Astrophys. J.* **1997**, *485*, 735. [CrossRef]
33. Philippov, A.A.; Cerutti, B.; Tchekhovskoy, A.; Spitkovsky, A. Ab Initio Pulsar Magnetosphere: The Role of General Relativity. *Astrophys J.* **2015**, *815*, L19. [CrossRef]
34. Daugherty, J.K.; Harding, A.K. Electromagnetic cascades in pulsars. *APJ* **1982**, *252*, 337–347. [CrossRef]
35. Usov, V.V.; Melrose, D.B. Pulsars with strong magnetic fields: Polar gaps, bound pair creation and nonthermal luminosities. *Aust. J. Phys.* **1995**, *48*, 571–612. [CrossRef]
36. Lomiashvili, D.; Machabeli, G.; Malov, I. On the Nature of Radio Pulsars with Long Periods. *Astrophys. J.* **2006**, *637*, 1010–1015. [CrossRef]
37. Kantor, E.M.; Tsygan, A.I. The Death Lines of Radio Pulsars for Dipolar and Asymmetric Magnetic Fields. *Astron. Rep.* **2004**, *48*, 1029–1036. [CrossRef]
38. Freire, P.C.; Camilo, F.; Kramer, M.; Lorimer, D.R.; Lyne, A.G.; Manchester, R.N.; D'Amico, N. Further results from the timing of the millisecond pulsars in 47 Tucanae. *Mon. Not. R. Astron. Soc.* **2003**, *340*, 1359–1374. [CrossRef]
39. Dowell, J.; Ray, P.S.; Taylor, G.B.; Blythe, J.N.; Clarke, T.; Craig, J.; Ellingson, S.W.; Helmboldt, J.F.; Henning, P.A.; Lazio, T.J.W.; et al. Detection and Flux Density Measurements of the Millisecond Pulsar J2145-0750 below 100 MHz. *Astrophys. J. Lett.* **2013**, *775*, L28. [CrossRef]
40. Beskin, V.S. General Relativity Effects on Electrodynamic Processes in Radio Pulsars. *Sov. Astron. Lett.* **1990**, *16*, 286.
41. Daugherty, J.K.; Harding, A.K. Gamma-Ray Pulsars: Emission from Extended Polar CAP Cascades. *Astrophys. J.* **1996**, *458*, 278. [CrossRef]

42. Yang, Y.P.; Zhang, B. Fast Radio Bursts and Their High-energy Counterparts from Magnetar Magnetospheres. *Astrophys. J.* **2021**, *919*, 89. [CrossRef]
43. Lyutikov, M. Escape of Fast Radio Bursts from magnetars' magnetospheres. *arXiv* **2021**, arXiv:2110.08435.